Springer

KSME

Journal of Mechanical Science and Technology 24 (12) (2010) 2545~2553
www.springerlink.com/content/1738-494x
DOI 10.1007/s12206-010-0914-2

Robust design of roll-formed slide rail using response surface method †

Minjin Oh[1], Moon Kyu Lee[2] and Naksoo Kim[2,*]

[1]*Mechanical Engineering Research and Development Laboratory, LIG Nex1 Co. Ltd, Korea*
[2]*Department of Mechanical Engineering, Sogang University, Seoul, 121-742, Korea*

(Manuscript Received March 15, 2010; Revised June 11, 2010; Accepted August 18, 2010)

Abstract

Roll-formed slide rail used as a linear guide in the smooth movement of drawers and electric home appliances requires geometric accuracy because of a high slenderness ratio and repetitive usage. The slide rail members are generally manufactured by the roll forming process. The members need to be improved through optimization of the roll forming process instead of the designer's experience. The aim of this study is to determine the optimal roll forming parameters by using robust optimization technique which simultaneously satisfies three criteria such as the shape difference factor, bowing factor and modified inverse safety factor. In analyzing the roll forming process of a slide rail, the pass in which the largest deformation occurred is designated as the target pass. The positions and the curvature of rolls are set as the design variables in the target pass. The cost function, which is comprised of the shape difference factor, the bowing factor, and the modified inverse safety factor, is obtained using design-of-experiments of the response surface method. The cost function is minimized by using robust optimization techniques and showed the improved the straightness and the durability value. Using robust design methodology, it is able to be constructed a multi-objective function, and optimized three criteria, simultaneously.

Keywords: Multi-objective function; Robust optimization; Roll forming; Table of orthogonal arrays

1. Introduction

A slide rail, which is comprised of several members and ball bearings, functions as a linear guide in the smooth movement of drawers and electric home appliances. A slide rail requires geometric accuracy for its sectional shapes, straightness, and durability since it requires a high slenderness ratio for a high degree of repetitive use. Slide rail members which produced by cold-rolled steel (SCP) stainless steel are manufactured through the roll forming process. Roll forming is a process that progressively bends a flat strip of sheet metal through many pairs of forming rolls, and provides the low-cost manufacturing for long sheet metal products of constant cross section.

Bhattacharayya et al. [1] performed a semi-empirical study, and by minimizing total energy produced an expression for predicting the deformation length of a channel section. Duggal et al. [2] compared finite element (FE) simulation results to Bhattacharayya's experimental results. Other numerical [3-6] and experimental [7-8] studies have been performed.

Designing a roll forming process of a slide rail has mainly relied on the designer's experience. Defects generated during the designing process are often identified after production of the prototype. In addition, the compatibility of the corrected design was verified after the reproduction of the prototype. This multiple process causes an increase in production cost and reduces the competitive production capability to the manufacturer. Recently a finite element (FE) simulation of the roll forming process has been used prior to the production of a prototype in order to predict the final shape of slide rail and diminishes the design defects might occurred .

Hong and Kim [9] developed a three-dimensional (3-D) FE simulation program of the roll forming process, and predicted scratch defects of the roll forming process using the finite element method. Their research employed the rigid-plastic finite element method to predict the edge shape [10] and roll wear [11]. Kim et al. [12] predicted buckling behavior in the roll forming process. Sheikh and Palavilayil [13] evaluated FE simulation programs such as SHAPE-RF. In addition, several studies have been reported the advantage of FE simulation programs in designing of roll forming process [14-17].

In this study, the accuracy of FE simulation was verified by comparing the shapes generated from the experimental results and simulation product. We suggest a shape difference factor (SDF) and a bowing factor (BF) as a standard for quantitative evaluating index which represents the quality of a formed shape and straightness respectively.

In a previous study, only the response surface method was

† This paper was recommended for publication in revised form by Associate Editor Youngseog Lee

* Corresponding author. Tel.: +82 2 705 8635, Fax.: +82 2 712 0799
E-mail address: nskim@sogang.ac.kr

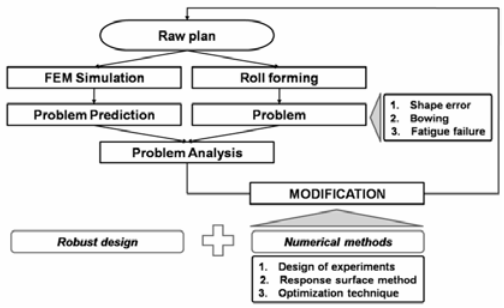

Fig. 1. Flow chart for the modification of the roll forming process design.

used in the optimization design of the shape difference factor to improve the geometric accuracy of the sectional shape [18]. The durability of the slide rail did not satisfy the standard value in the fatigue test. The FE simulation provided the prediction of manufacturing condition of fatigue life which similar to that produced under experimental situation. A critical factor, the tensile residual stress, influencing the fatigue failure of the product generated after the roll forming process was identified by using modified inverse safety factor (MISF) as a correcting factor. Thus, the goal of this study is to design optimal roll forming parameters by using the robust optimization design technique which provide the reliable values of the shape difference factor, the bowing factor, and the modified inverse safety factor that satisfy criterion of each factor.

2. Critical factors of the slide rail

Design variables at the roll forming pass with the maximally deformed slide rail were defined as a roll location and a geometric curvature to perform multi-objective optimization of a slide rail for geometric precision, straightness and durability. Three criteria, the shape difference factor (SDF), bowing factor (BF), and modified inverse safety factor (MISF), were determined from the design variables and the objective functions, and were calculated by using a table of orthogonal arrays based on the statistical response surface method (RSM), as shown in Fig. 1.

2.1 Shape Difference Factor (SDF)

A slide rail which structured with complicated shape and requires a high degree of precision is manufactured by using the roll forming process [19]. It is difficult to determine the compatibility with the design because the product has a complicated cross-sectional shape. Therefore, a standard is necessary to quantitative evaluation of the quality of the formed shape; one of the proposed value suggested in this study is the shape difference factor (SDF).

In order to quantitatively evaluate the precision of the shape of a slide rail member manufactured by the roll forming process, the cross-section of an FE simulation model or data from an experimental result is set on the center of a cross-section of

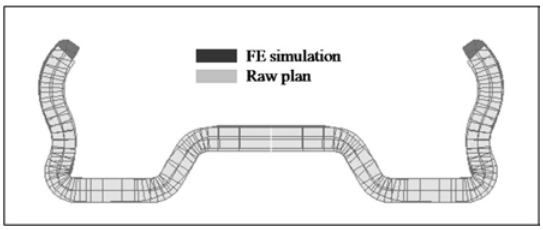

Fig. 2. Comparison of FE simulation model and raw plan.

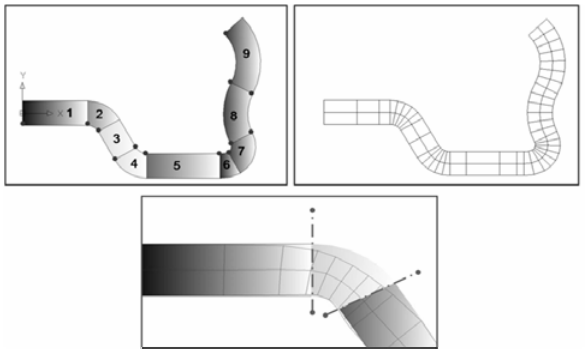

Fig. 3. Area calculation between the raw plan and FE simulation model.

a raw plan with grids drawn on it, as shown in Fig. 2. As shown in Fig. 3, the raw plan was divided into nine sections. SDF was calculated by the summation of the difference in the measured area between the raw plan and the simulation or experimental result at every section, as follows:

$$y = \beta_0 + \sum_{i=1}^{n_d} \beta_i x_i + \sum_{i=1}^{n_d} \sum_{j \geq i}^{n_d} \beta_{ij} x_i x_j \quad (1)$$

where A_i denotes the cross-sectional area of FE simulation result or experimental result at the i^{th} section, and A_{i0} denotes the sectional area of the raw plan at the i^{th} section. Because the cross-sectional shape of the product is symmetric, SDF is measured at the right cross section of the product.

2.2 Bowing Factor (BF)

Bowing or twist of roll-formed products can appear since the residual stress is accumulated through the roll forming process (Fig. 4). Fig. 4 shows the bowing amount (a), the result of forming analysis at 25th stand as the final step of roll forming process (b) and the shape of the final strip measuring the bowing amount (c). Particularly Fig. 4(b) indicates the bowing is represented after the strip passes the center (center line) of the roll. The amount of the bowing should be minimized for the smooth shuttling of the product which uses the slide rail. A standard called the bowing factor (BF) is necessary for quantitative evaluation of the straightness and is defined as follows:

$$\mathrm{BF} = h/t_0 \quad (2)$$

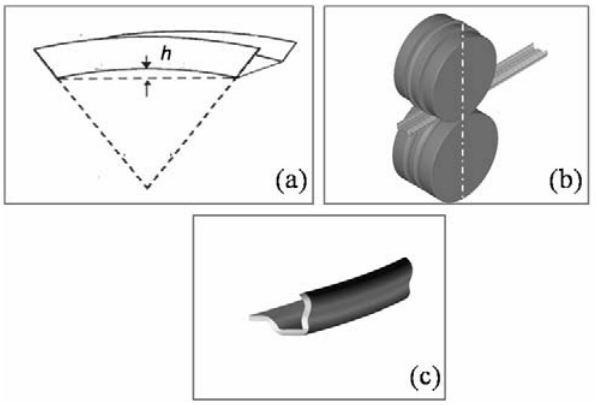

Fig. 4. Schematics represent the definition of bowing.

where h denotes the maximum bowing quantity from the FE simulation or experimental result, and t_0 denotes the thickness of the initial shape.

2.3 Modified Inverse Safety Factor (MISF)

The roll forming process causes a plastic deformation of slide rail. Internal void growth occurs and causes a ductile fracture when plastic deformation occurs. Ragab [20] proposed a ductile fracture criterion as shown in Eq. (3) which was able to validate by experiment:

$$\frac{\sigma_n}{\bar{\sigma}_M}=\left(1+\frac{2\lambda_1^2}{b_2/b_1-1}\right)\log\left[1+\frac{1}{2\lambda_1^2}(b_2/b_1-1)\right]X\left[1-\frac{\pi}{4}\left(\frac{b_1}{b_2}\right)^2\right](\varepsilon_l/\varepsilon_{uc})^n$$
$$b_1/b_2=\left(6\lambda_2 f/\pi\lambda_1\right)^{1/3} \quad (3)$$

where σ_n is the plastic-limit load stress, $\bar{\sigma}_M$ is the matrix effective flow stress within the ligament, ε_l is the average macroscopic strain within the ligament, ε_{uc} is the average macroscopic strain for the unit cell, λ_1 is the current void aspect ratio, λ_2 is the current aspect ratio of the unit cell, b_1 is the length of the semi-minor axis of void whose shape is ellipse, b_2 is the length of the shorter side of cell and f is the current void fraction. This equation was used in calculating the strain when the fatigue failure occurs.

Kanvinde and Deierlein [21] proposed a periodic void growth model of low cycle fatigue with ductile fracture. They described the relationship in Eq. (4) which shows that the cyclic damage parameter λ has a value of 0.4~0.5 for steel. The damage ratio becomes smaller with increasing cumulative strain. Thus, we have

$$\text{Damage ratio}=\frac{\text{VGI}_{\text{cyclic}}^{\text{critical}}}{\text{VGI}_{\text{monotonic}}^{\text{critical}}}=\exp(-\lambda\varepsilon_p^{accumulated}) \quad (4)$$

where $\text{VGI}_{\text{cyclic}}^{\text{critical}}$ is the critical cyclic void growth index, $\text{VGI}_{\text{monotonic}}^{\text{critical}}$ is the critical monotonic void growth index, and $\varepsilon_p^{accumulated}$ is the cumulated plastic strain.

It is necessary to decreases the tensile residual stress of the cross-section of the product since the tensile residual stress might induce undesirable influence on the life cycle of the product. To evaluate quantitatively the influence of the tensile residual stress for the fatigue life, a modified inverse safety factor (MISF), shown in Eq. (5), was used and defined as the safety factor of the Goodman line considering the tensile residual stress and the damage ratio. λ was set to 0.45. Thus,

$$\text{MISF}=\frac{\varepsilon_f^{accumulated}}{\varepsilon_{frac}}+\frac{1}{\exp(-\lambda\varepsilon_f^{accumulated})}x\left(\frac{1}{n_f}+\frac{residual\ stress}{S_{ut}}\right)a \quad (5)$$

where $\varepsilon_f^{accumulated}$ is the accumulated plastic strain, ε_{frac} is the strain when the fatigue failure occurs, n_f is the safety factor of the Goodman line, and S_{ut} is the ultimate tensile strength.

Table 1. Roll forming process condition of FE simulation.

Material property	Flow stress (MPa)	$\sigma_f=502(0.002+\bar{\varepsilon})^{0.024}$
	Young's modulus (GPa)	210
	Poisson's ratio	0.3
	Yield strength (MPa)	433
	UTS (MPa)	460
Initial thickness (mm)		2.0
Strip width (mm)		60.0
Friction coefficient		0.1

3. Simulation

3.1 Roll forming process condition

A slide rail is comprised of an inner member, middle member, outer member, and ball bearings. We focused on the role of the middle member by which an inner rail and an outer rail are connected requires a high precision for the operation of a slide rail.

The middle member is manufactured with a 25-pass line. The distance between the passes is 350 mm; odd-numbered passes are set up as driving rolls, even-numbered passes are set up as idle rolls, all rolls are modeled as rigid body and the velocities of each pass roll are set to produce a product with a constant velocity of 40 m/min. The thickness and width of the initial strip is 2 mm and 60 mm, respectively; the strip is made of SCP10 whose material properties are listed in Table 1.

3.2 FE simulation program

FE simulations are performed by using the roll forming simulation program SHAPE-RF v4.0.0 which is based on the rigid-plastic finite element method. This program adopts the normalized plane strain condition as the initial boundary condition for initially determining the free surface. The velocity field was calculated by FEA of the 3-D kinematic steady state, and the final shape was determined by an iterative method that calibrates the boundary conditions and the free surface. The strain rate and pressure torque is obtained based on the veloc-

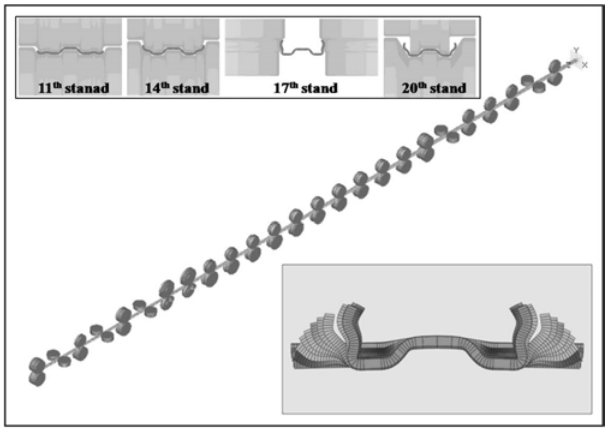

Fig. 5. Roll forming process embodied in FE simulation.

ity field and the effect of the elastic recovery is considered by the supplementary module of the elastic analysis in this program. The reliability of SHAPE-RF has been verified in several previous papers [9-13].

Swift's flow stress equation was used to express the stress-strain relation of a strip, and is defined as follows:

$$\sigma_f = K(\overline{\varepsilon}_0 + \overline{\varepsilon})^n \tag{6}$$

where σ_f denotes the flow stress, K is the strength coefficient, $\overline{\varepsilon}$ is the effective strain, $\overline{\varepsilon}_0$ is the initial effective strain, and n is the strain hardening coefficient. The flow stress of the strip was obtained by using the "convert" function of SHAPE-RF and is shown in Table 1. The flower pattern (the shape profile at each pass in the roll forming process) of the middle member was obtained by using the FE simulation program, and is shown in Fig. 5.

3.3 Verification of FE simulation

3.3.1 Shape precision

The SDF values obtained from the experimental and simulation results are 0.478 and 0.489, respectively. The difference between the results and the raw plan occurred possibly in the regions where the slide rail was bent. The average difference in area between the experimental results and the raw plan is 1.18 mm^2. The difference in SDF between the FE simulation and the experimental results is small and appeared as the value of 2.25%.

3.3.2 Quantity of Bowing

We measured the quantity of bowing by using a thickness gauge and a 3-D shape measuring instrument. The results obtained from two experimental machines are shown in Table 2. The average of the value was 0.61 mm. The BF obtained from the experimental results was 0.305 and the quantity of bowing from FE simulation was 1.89 mm. The result indicated the relatively small difference since the unit length of the measurement is 100 mm. Therefore, it would be conclude that the FE simulation is desirable method to predict an approximate value of bowing.

Table 2. Measurement of bowing (unit : mm).

Methods \ Number	1	2	3	4	5
Thickness Gauge	0.70	0.60	0.70	0.85	0.60
3D shape measuring instrument	0.50	0.35	0.67	0.56	0.52

Methods \ Number	6	7	8	9	10
Thickness Gauge	0.70	0.80	0.50	0.70	0.70
3D shape measuring instrument	0.59	0.59	0.46	0.59	0.53

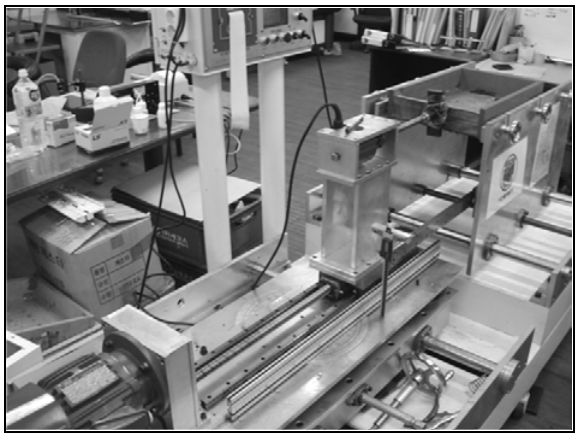

Fig. 6. Durability testing machine.

3.3.3 Durability

In the initial model, a fatigue load of 589 N was applied to the end position of the inner member linked in the fixed outer member to evaluate the durability of the slide rail using a durability testing machine (Fig. 6). The middle member shown the fracture when the load cycles reached on 130,000 from the criterion cycles of 150,000 (Fig. 7). The stress amplitude in the fatigue analysis is defined as the half of the maximum stress which is obtained by the static load applied at each member of the slide rail. Then, the worst-case of the fatigue simulation was performed for the middle member, which was applied from the tensile residual stress of the roll forming simulation using the commercial program of ANSYS ver. 10.0 (Fig. 8(a)).

The simulation results showed that the maximum stress occurred in the middle member with the fatigue life of 157,320 cycles which calculated based on the Goodman criterion (Fig. 8(b)). The result of the fatigue life test showed the value of error about 21% when the fatigue load was applied as a static maximum load for the simulation condition. Thus, this simulation condition of loading maximum static load for fatigue loading would generate the reliable prediction for the location of fatigue fracture when compared to that produced by con-

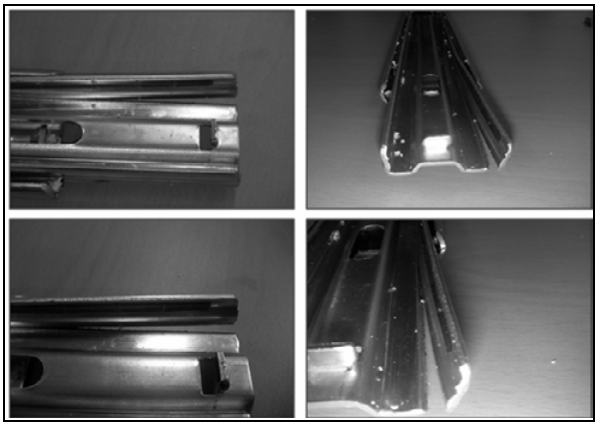

Fig. 7. Fracture generated in middle member of slide rail following the durability test.

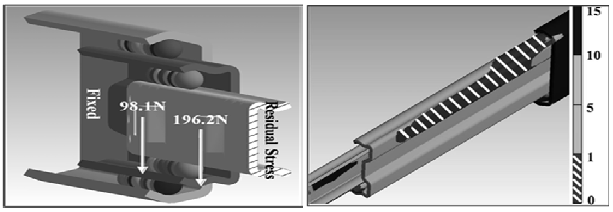

(a) (b)

Fig. 8. Boundary condition and FE simulation result: (a) Boundary condition; (b) Safety factor distribution.

ventional durability testing machine.

4. Optimal design of the slide rail

4.1 Designation of target pass and design variables

The design-of-experiments faces the limitation of the design range since many design variables such as a roll velocity, the distance between rolls, and geometric parameters at each roll. These variables are closely related and their well-organized function is required for the generation of the roll forming process. The 18th roll pass is determined as the target pass through the finite element simulation that reveals the maximum longitudinal strain occurred in the middle member of the slide rail.

Three design variables are defined as the *x* coordinates at the range of straight line (A), the *y* coordinates of the same line (B), and the radius of curvature at the right roll (C) in the symmetric geometry of 18th pass (Fig. 9). Table 3 shows three levels of design variables.

4.2 Optimal design for SDF

An orthogonal-array table $L_9(3^4)$ was constructed using an allegation orthogonal-array table. The SDF result was obtained by using a finite element program, SHAPE-RF Ver. 4.0 (Korea), to obtain the data for the orthogonal-array table (Table 4). The objective function of SDF is constructed by the

Table 3. Level of the design variables (unit : mm).

Design Variables	Level 0	Level 1	Level 2
A	17.7	18.7	19.7
B	12.56	13.56	14.56
C	5	5.4	5.8

Table 4. Tables of orthogonal arrays for SDF.

Exp. No.	A	B	C	SDF of simulation
1	0	0	0	0.480
2	0	1	1	0.421
3	0	2	2	0.384
4	1	0	2	0.444
5	1	1	0	0.463
6	1	2	1	0.377
7	2	0	1	0.431
8	2	1	2	0.416
9	2	2	0	0.455

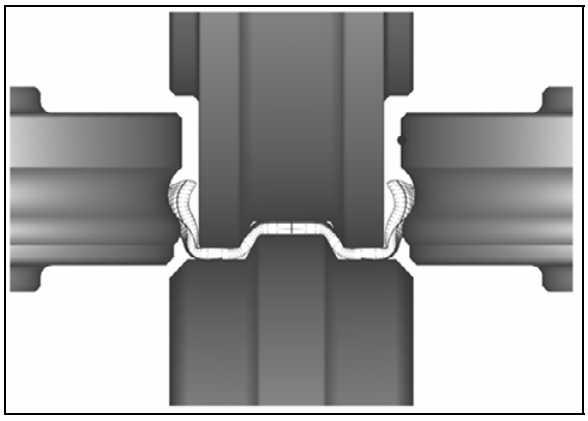

Fig. 9. Simulation result shows the Shape of 18th stand.

surface response method as follows:

$$\begin{aligned}\Phi_1 = {} & 6.621 - 0.388X_1 + 0.351X_2 - 1.659X_3 \\ & + 0.011X_1^2 - 0.005X_2^2 + 0.198X_3^2 \\ & - 0.002X_1X_2 - 0.040X_2X_3\end{aligned} \tag{7}$$

The objective function was validated by the simulation results for the data in Table 4. The results showed the reasonable error value of 5.75% when calculated by using Eq. (8):

$$\text{Error}(\%) = \frac{\left|\Phi^c - \Phi^a\right|}{\Phi^c} \times 100 \tag{8}$$

where Φ^c is the value of SDF from each simulation, and Φ^a is the value of SDF for the design variables from the objective function which generated by the response surface method. Therefore, it would be concluded that this objective function might exactly indicate the difference between the ideal geometry and the predicted final geometry in 18th pass.

Table 5. Tables of orthogonal arrays for BF.

Exp. No.	A	B	C	BF of simulation
1	0	0	0	0.859
2	0	1	1	1.050
3	0	2	2	1.882
4	1	0	2	0.702
5	1	1	0	1.203
6	1	2	1	0.954
7	2	0	1	0.950
8	2	1	2	0.737
9	2	2	0	0.689

The objective function was minimized by the method of Broyden-Fletcher-Goldfarb-Shanno (BFGS) which directly updates the Hessian matrix. The result shows that the optimal values of A (X_1), B (X_2), C (X_3), and the cost function (Φ_1) are 19.7, 14.56, 5.65 and 0.29. The finite element simulation result for these optimal values is 0.365, and is smaller than the initial value of 0.489. The reason for the error between Φ^c and Φ^a is resulted from the objective function which constructed by the limited design variables in the target pass.

4.3 Optimal design for BF

This optimal design also uses the orthogonal array table $L_9(3^4)$, and Table 5 shows the simulation results for BF. The objective function of SDF using the surface response method is given in Eq. (9).

$$\begin{aligned}\Phi_2 = & -42.634 + 4.375X_1 + 8.682X_2 - 20.164X_3 \\ & + 0.057X_1^2 + 0.009X_2^2 + 1.718X_3^2 \\ & - 0.495X_1X_2 + 0.091X_2X_3\end{aligned} \quad . \quad (9)$$

The objective function was validated by the results of the simulation as shown in Table 5. The computed error showed the reasonable value of 5% according to Eq. (8), where Φ^c is the value of BF from each simulation condition and Φ^a is the value of BF for the design variables from the objective function when the response surface method was used. As result, this objective function might acceptable for e the prediction of bowing amount in the 18th pass.

The objective function was minimized by the method of BFGS. The result shows the optimal values of A (X_1), B (X_2), C (X_3) and the cost function (Φ_2) showed the values of 19.7, 14.56, 5.48 and 0.365. These optimal values generated from the finite element simulation were appeared as 0.437, which is smaller than the initial value of 0.945.

4.4 Optimal design for MISF

Fig. 10(a) shows the tensile residual stress obtained from the computing with the finite element program, SHAPE-RF Ver. 4.0 (Korea) to measure the data of the orthogonal-array (Table 6). The tensile residual stress was extracted from 82 points of cross section, as shown in Fig. 10(b). The residual stresses can be obtained after the roll forming process was completed by calculating the principal stresses which is converted from that of actual stresses measured at the strip section. The objective function of MISF based on the tensile residual stress and the plastic strain was constructed by the surface response method (Eq. (10)).

Table 6. Tables of orthogonal arrays for MISF.

Exp. No.	A	B	C	MISF of simulation
1	0	0	0	2.521
2	0	1	1	2.499
3	0	2	2	3.715
4	1	0	2	4.310
5	1	1	0	4.786
6	1	2	1	3.329
7	2	0	1	3.437
8	2	1	2	3.889
9	2	2	0	3.771

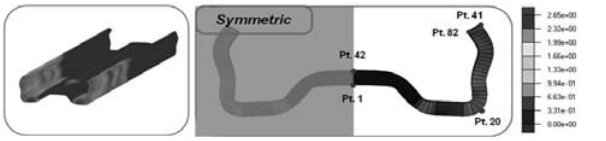

(a) (b)

Fig. 10. Residual stress after roll forming: (a) Residual stress; (b) Points to extract the tensile residual stress.

$$\begin{aligned}\Phi_3 = & -317.461 + 36.259X_1 + 23.317X_2 - 65.973X_3 \\ & - 0.696X_1^2 - 0.211X_2^2 + 6.939X_3^2 \\ & - 0.733X_1X_2 - 0.701X_2X_3\end{aligned} \quad . \quad (10)$$

The objective function was validated by the results of the simulation for the data in Table 6. The determined error showed the reasonable value of about 5% computed by using Eq. 8, where Φ^c is the value of MISF from each simulation and Φ^a is the value of MISF for the design variables from the objective function using the response surface method. Therefore, it would be expected that this objective function could provide the reliable MISF which is related to the fatigue life in the 18th pass.

The objective function was minimized when the BFGS method was used for determination. The results shows the optimal values of A (X_1), B (X_2), C (X_3), and the cost function (Φ_3) as 19.7, 14.56, 5.49, and 2.137. The result obtained from the finite element simulation for these optimal values was 2.479, which is smaller than the initial value of 2.878.

4.5 Robust design including multiple objective functions

Table 7 shows the orthogonal array table $L_9(3^4)$ used for obtaining the robust design. For the simulation, each variable which divided into three levels from the initial value with

Table 7. Tables of orthogonal arrays for robust design.

Exp. No.	A	B	C	SDF Avg.	SDF S.D.	BF Avg.	BF S.D.	MISF Avg.	MISF S.D.
1	0	0	0	0.443	0.037	0.893	0.034	2.501	0.020
2	0	1	1	0.377	0.043	1.082	0.032	2.491	0.008
3	0	2	2	0.334	0.051	1.911	0.029	3.719	0.004
4	1	0	2	0.410	0.035	0.744	0.042	4.321	0.011
5	1	1	0	0.419	0.043	1.239	0.036	4.790	0.004
6	1	2	1	0.327	0.051	0.987	0.033	3.344	0.015
7	2	0	1	0.400	0.035	0.998	0.048	3.459	0.022
8	2	1	2	0.375	0.042	0.782	0.045	3.923	0.034
9	2	2	0	0.405	0.051	0.727	0.038	3.798	0.027

(Tolerance : $\pm$ 0.1)

Table 8. Tables of orthogonal arrays for robust design.

Scale	1	2	3	4	5	6	7	8
No. of terms used	2	3	4	5	6	7	9	11
1. Extremely high								0.954
2. Very high			0.909		0.917	0.909	0.917	0.864
3. High -Very high							0.875	0.701
4. High	0.750	0.833	0.717	0.885	0.750	0.773	0.750	0.667
5. Fairty high				0.700	0.584		0.630	
6. Moi high						0.637		0.590
7.Medium	0.583	0.500	0.500	0.500		0.500	0.500	0.500
8. Moi low						0.363		0.410
9.Fair low				0.300	0.416		0.370	
10. Low		0.166	0.283	0.115	0.250	0.227	0.250	0.333
11. Low – Very low							0.125	0.299
12. Very low			0.091		0.083	0.091	0.083	0.136
13. None								0.046

range of $\pm$ 0.1 was employed. The simulation of each variable set was performed, and this result was used to construct a multi-objective function with weighting factors for calculating the SDF, BF and MISF based on the fuzzy number (Table 8). In this study, six fuzzy numbers were selected as values corresponding to that of the intuitive factors indicating very high, medium, low, very low, moi high and moi low (Eq. (11)).

$$\Phi = 0.909\left(\frac{\mu_{SDF}}{\mu_{SDF0}}\right) + 0.5\left(\frac{\sigma_{SDF}}{\sigma_{SDF0}}\right) + 0.227\left(\frac{\mu_{BF}}{\mu_{BF0}}\right) + 0.091\left(\frac{\sigma_{BF}}{\sigma_{BF0}}\right) + 0.637\left(\frac{\mu_{MISF}}{\mu_{MISF0}}\right) + 0.363\left(\frac{\sigma_{MISF}}{\sigma_{MISF0}}\right) \quad (11)$$

where μ_{SDF0}, σ_{SDF0}, μ_{BF0}, σ_{BF0}, μ_{MISF0}, σ_{MISF0} are, the standard value of the average and the deviation in SDF, BF, and MISF. Eq. (12) shows the multi-objective function applied to calculate the average values:

$$\Phi = 0.909\left(\frac{\mu_{SDF}}{0.387}\right) + 0.5\left(\frac{\sigma_{SDF}}{0.043}\right) + 0.227\left(\frac{\mu_{BF}}{1.040}\right) + 0.091\left(\frac{\sigma_{BF}}{0.037}\right) + 0.637\left(\frac{\mu_{MISF}}{3.594}\right) + 0.363\left(\frac{\sigma_{MISF}}{0.016}\right) \quad (12)$$

Table 9. Tables of orthogonal arrays for SDF.

Criterion Factor	Initial value	Simple optimization	Robust optimization
Shape difference factor (SDF)	0.489	0.365	0.361
Bowing factor (BF)	0.945	0.437	0.587
Modified inverse safety factor (MISF)	2.878	2.479	2.362

Finally, the multi-objective function was minimized by the using the BFGS method. The results showed that the optimal values of A (X_1), B (X_2), C (X_3), and the cost function (Φ) were 19.7, 14.56, 5.54, and 324.5.

The FE simulation results of the optimal values of the 18th roll pass were 0.361 in SDF, 0.587 in BF, and 2.362 in MISF (Table 9).

The minimum value of objective function generated by using the robust design based on the multiple objective functions showed a little discrepancy with that obtained from the minimum value of SDF, BF and MISF. However, the geometric precision, straightness and durability of the slide rail resulted from the robust design showed their improved property when compared to those of previous result.

5. Conclusion

In this study, the robust design technique in roll forming process of slide rail members showed the improved properties of multiple objective functions representing shape precision, straightness, and durability. Thus we propose and summarize our conclusions as follows:

(1) The correction of specified target roll pass by measuring the longitudinal strain influenced the degree of shape precision and straightness in the roll forming process.

(2) A shape difference factor (SDF), a bowing factor (BF), and a modified inverse safe factor (MISF) in the slide rail function as the criteria for optimal design. Their objective functions were derived from the experimental design method, especially, the response surface method.

(3) Following our improved process, the cost functions of SDF, BF, and MISF showed the decreased value of 25.36%, 53.76%, and 13.86% than their previous design values. These results support the notion that the shape precision, the straightness, and the durability of the slide rail in the finite element simulation were improved when the robust design of the response surface method was used.

Nomenclature

A : Cross sectional area
f : Current void fraction
h : Maximum bowing amount
K : Strength coefficient
$L_N(2^k)$: Table of orthogonal arrays
n : Strain hardening coefficient
n_{f_f} : Safety factor of Goodman line
S_{ut} : Ultimate tensile strength
t_0 : Thickness of initial strip
λ : Cyclic damage parameter
λ_1 : Current void aspect ratio
λ_2 : Current aspect ratio of the unit cell
σ : Stress
σ_f : Flow stress
Φ^c : SDF, BF and MISF computed from each simulation
Φ^a : Value of the cost function when the same variables are inputted

References

[1] D. Bhattacharayya, P. D. Smith, C. H. Yee and I. F. Collins, The prediction of Deformation length in cold roll forming, *J. Mech. Working Technol.*, (9) (1984) 181-191.

[2] N. Duggal, M. A. Ahmetoglu, G. L. Kinzel and T. Altan, Computer aided simulation of cold roll forming-a computer program for simple section profiles, *J. Mater. Proc. Technol.*, (59) (1996) 41-48.

[3] M. Brunet and S. Ronel, Finite element analysis of roll-forming of thin sheet metal, *J. Mater. Proc. Technol.*, (45) (1994) 255-260.

[4] M. Brunet, B. Lay and P. Pol, Computer aided design of roll-forming of channel sections, *J. Mater. Proc. Technol.*, (60) (1996) 209-214.

[5] C. Liu, Y. Zhou and W. Lu, Numerical simulation of roll-forming by B-spline finite strip method, *J. Mater. Proc. Technol.*, (60) (1996) 215-218.

[6] M. Farzin, M. S. Tehrani and E. Shameli, Determination of buckling limit of strain in cold roll forming by the finite element analysis, *J. Mater. Proc. Technol.*, (2002) 125-126, 626-632.

[7] S. M. Panton, J. L. Duncan and S. D. Zhu, Longitudinal and shear strain development in cold roll forming, *J. Mater. Proc. Technol.*, (60) (1996) 219-224.

[8] M. Lindgren, Experimental investigations of the roll load and roll torque when high strength steel is roll formed, *J. Mater. Proc. Technol.*, (191) (2007) 44-47.

[9] S. Hong and N. Kim, Study on scratch defect of roll forming process, *Trans. of the KSME* (A), (25) (2001) 1213-1219.

[10] S. Lee and N. Kim, Prediction and design of edge shape of initial strip for thick tube roll forming using finite element method, *Trans. of the KSME* (A), (26) (2002) 644-652.

[11] B. Kang and N. Kim, A study on roll wear in the roll forming process, *Trans. of the KSME* (A), (27) (2003) 644-652.

[12] Y. Kim, J. Kim, Y. Jeoung and N. Kim, Buckling analysis of roll forming process using finite element method, *Trans. of the KSME* (A)., (27) (2003) 1451-1456.

[13] M. A. Sheikh and R. R. Palavilayil, An assessment of finite element software for application to the roll-forming process, *J. Mater. Proc. Technol.*, (180) (2006) 221-232.

[14] A. Alsamhan, P. Hartely and I. Pillinger, The computer simulation of cold-roll-forming using FE methods and applied real time re-meshing techniques, *J. Mater. Proc. Technol.*, (142) (2003) 102-111.

[15] A. K. Datta, G. Das, P. K. De, P. Ramachandrarao and M. Mukhopadhyaya, Finite element modeling of rolling process and optimization of process parameter, *Material Science and Engineering* (A)., (426) (2006) 11-20.

[16] M. Lindgren, Cold roll forming of a U-channel made of high strength steel, *J. Mater. Proc. Technol.*, (186) (2007) 77-81.

[17] R. S. Senanayake, I. M. Cole and S. Thiruvarudchelvan, The application of computational and experimental techniques to metal deformation in cold roll forming, *J. Mater. Proc. Technol.*, (45) (1994) 155-160.

[18] M. Oh and N. Kim, Optimum design of roll forming process of slide rail using design of experiments, *J. of Mech. Science and Technol.,* 2008, 22, 1537-1543.

[19] S. Jeong, S. Lee, G. Kim, J. Kim and S. Shin, Rigid-plastic finite element method for development mold of dishwasher's under rail roll forming, *Trans. of the KSMPE Annual Meeting.*, (2006) 644-652.

[20] A. R. Ragab, A model for ductile fracture based on internal necking of spheroidal voids, *Acta Materialia*, (52) (2004) 3997-4009.

[21] A. M. Kanvinde and G. G. Deierlein, Cyclic void growth model to assess ductile fracture initiation in structural steels due to ultra low cycle fatigue. J. of engineering mechanics-ASCE, (2007) 701-712.

Minjin Oh received his B.S. and M.S. degree from the department of Mechanical Engineering, Sogang University, Seoul, S. Korea in 2007 and 2009, respectively. Mr. Oh is currently working for LIG Nex1. His research interests are in the area of optimum design of metal forming, and process design.

Moon Kyu Lee received his B.S. and M.S. degree from the department of Mechanical Engineering, Sogang University, Seoul, S. Korea in 1999 and 2001, respectively. He then went on to receive his Ph. D. degree from Sogang University in 2007. Dr. Lee had worked for Korea Automobile Testing & Research Institute as a senior researcher. He is currently a research professor at the department of mechanical engineering, Sogang University. His research interests are in the area of optimum design of mechanical components.

Naksoo Kim received his B.S. and M.S. degree from the department of Mechanical Design, Seoul National University in 1982 and 1984, respectively. He then went on to receive his Ph. D. degree from U.C. Berkeley. Dr. Kim had worked for the ERC/NSM at the Ohio State University as a senior researcher and Hongik University as an assistant professor. He is currently a professor at the department of mechanical engineering, Sogang University. Dr. Kim's research interests are in the area of metal forming plasticity, computer aided process analysis, and optimal design.